

A new standardized Palmer drought index for hydro-meteorological use

Mingwei Ma,^{1,2} Liliang Ren,^{1,2*} Fei Yuan,^{1,2} Shanhui Jiang,^{1,2} Yi Liu,^{1,2} Hao Kong² and Luyan Gong²

¹ State Key Laboratory of Hydrology-Water Resources and Hydraulic Engineering, Hohai University, Nanjing 210098, China

² College of Hydrology and Water Resources, Hohai University, Nanjing 210098, China

Abstract:

Accepting the concept of standardization introduced by the standardized precipitation index, similar methodologies have been developed to construct some other standardized drought indices such as the standardized precipitation evapotranspiration index (SPEI). In this study, the authors provided deep insight into the SPEI and recognized potential deficiencies/limitations in relating to the climatic water balance it used. By coupling another well-known Palmer drought severity index (PDSI), we proposed a new standardized Palmer drought index (SPDI) through a moisture departure probabilistic approach, which allows multi-scalar calculation for accurate temporal and spatial comparison of the hydro-meteorological conditions of different locations. Using datasets of monthly precipitation, temperature and soil available water capacity, the moisture deficit/surplus was calculated at multiple temporal scales, and a couple of techniques were adopted to adjust corresponding time series to a generalized extreme value distribution out of several candidates. Results of the historical records (1900–2012) for diverse climates by multiple indices showed that the SPDI was highly consistent and correlated with the SPEI and self-calibrated PDSI at most analysed time scales. Furthermore, a simple experiment of hypothetical temperature and/or precipitation change scenarios also verified the effectiveness of this newly derived SPDI in response to climate change impacts. Being more robust and preferable in spatial consistency and comparability as well as combining the simplicity of calculation with sufficient accounting of the physical nature of water supply and demand relating to droughts, the SPDI is promising to serve as a competent reference and an alternative for drought assessment and monitoring. Copyright © 2013 John Wiley & Sons, Ltd.

KEY WORDS drought indices; water balance; probability distribution; standardization; Palmer; climate change

Received 6 March 2013; Accepted 9 September 2013

INTRODUCTION

Droughts are hydro-meteorological anomalies characterized by prolonged deficit in regional water budget and could cause temporary difficulties (even failures) in water supply. Today, more severe droughts are breaking out in frequency, magnitude and duration with constantly increasing water consumption, inducing serious and far-reaching socio-economic and eco-environmental problems worldwide (Ma *et al.*, 2013). As such frequent drought suffering, great efforts have been made to meet the need of more accurate evaluations for better decision-making in drought prevention and mitigation. And the most successful attempts among these practices might be the development and the use of various objective indices. For example, the Palmer drought severity index (PDSI) and standardized precipitation index (SPI) are two of the

most outstanding models being frequently used for improving the detection of drought's onset and closure, as well as quantifying other critical features of this phenomenon.

The PDSI introduced by Palmer (1965) is a landmark in the development of drought indices, and it considers a range of factors that could pose an impact on drought (e.g. prior precipitation, water supply, soil moisture recharge, run-off and land surface evaporation demand). Over the past half-century since its birth, the PDSI has been widely used and become a standard for measuring droughts (e.g. Cook *et al.*, 1999; Dai *et al.*, 2004). However, Alley (1984) examined the structure of the PDSI and concluded that it used rather arbitrary rules in quantifying drought properties and drought classification and was spatial-temporally difficult for accurate comparisons because of limitations in the methodology used to standardize the values of PDSI for different locations and months. Another review conducted by Heddinghaus and Sabol (1991) drew similar conclusions. Wells *et al.* (2004) adopted an automatically calculating procedure to develop the self-calibrated PDSI (SC-PDSI), which had

*Correspondence to: Liliang Ren, State Key Laboratory of Hydrology-Water Resources and Hydraulic Engineering, Hohai University, No. 1 Xikang Road, Nanjing 210098, China.
E-mail: RLL@hhu.edu.cn

improved the spatial comparability of PDSI among diverse climatological regions (Alley, 1984; Guttman *et al.*, 1992). But even so, potential problems of the PDSI in relating to its arbitrary designation of drought severity classes and internal temporal memory (between 9 and 12 months) remain unsolved (Guttman, 1998), and the unchanged approximation of climatic characteristic using an empirically semi-logarithmic regression method still depends heavily on other reference locations and data (refer to the empirical constants in formula (1) of Wells *et al.* (2004), same as in formula (26) of Palmer (1965)). On the other hand, McKee *et al.* (1993) clearly illustrated multi-scalar nature of droughts and developed the SPI through a precipitation probabilistic approach to address temporal scale problems suffered by the PDSI. Using a given distribution (e.g. gamma) to fit the empirical frequency of precipitation data series, the SPI can be calculated at different time scales through numerical approximation standardization, which allows it readily comparable in time and space (Guttman, 1998; Hayes *et al.*, 1999). As a simple multi-scalar drought index, it obtained wide acceptance and was applied for monitoring droughts and managing different usable water resources (e.g. Guttman, 1999; Lloyd-Hughes and Saunders, 2002). Nevertheless, there were also many criticisms of the SPI behind its popularity. The most common complaints are that its calculation is based purely on precipitation observations, and the index does not consider other variables that can actually influence droughts, such as evaporation and soil moisture.

Understanding that the concept employed by McKee *et al.* (1993) for calculating SPI is more a mathematical approach developed to transforming skewed distributions into Gaussian (normal) form than merely a unique meteorological drought indicator and the procedure can be applied to any other variables relevant to drought (including some conceptual variables defined by well-founded water balance equations), Vicente-Serrano *et al.* (2010a) proposed the standardized precipitation evapotranspiration index (SPEI), which included temperature data in its formulation. In their proposal, the derived water difference [precipitation minus potential evapotranspiration (PET)] series was represented by a theoretical three-parameter log-logistic (LLG) distribution before being standardized to obtain expected SPEI values for evaluating drought. The SPEI was declared to combine the sensitivity of PDSI to changes in evaporation demand caused by temperature fluctuations/trends with the simplicity of calculation and the multi-temporal nature of SPI. A number of literatures show its recent applications (e.g. Lorenzo-Lacruz *et al.*, 2010; Vicente-Serrano *et al.*, 2010b; Paulo *et al.*, 2012).

Although incorporating the effect of temperature variability (in terms of PET) on drought evaluation and relieving long criticism of the SPI's basing only on

precipitation data, the SPEI is not granted as perfect and does have potential limitations, especially with respect to the water balance and water difference it used for measuring monthly water surplus/deficit conditions. Thus, following this brief introduction, the present study first attempts to figure out some critical drawbacks of the climatic water balance adopted by the SPEI compared with that defined by the PDSI. Our second objective is to follow procedures of the SPI/SPEI and to propose a new standardized Palmer drought index (SPDI) through a moisture departure probabilistic approach coupling the Palmer drought mode. On the basis of relevant comparisons of the SPI/SPEI, SPDI and SC-PDSI time series for 11 meteorological stations from different climate divisions, some discussions and conclusions are achieved in the end.

PROBLEMS AND REMEDY

In order to illustrate the problem in calculation of the SPEI and potential limitations in its application, we still selected most of the stations used by Vicente-Serrano *et al.* (2010a) for the initial development of the SPEI. However, although trying to use the same data for more convincing comparison, we could not manage to obtain complete precipitation and temperature datasets of Valencia (Spain) anyway. Alternatively, we have to adopt the other WMO gauging station in Athens (Greece) located in the same Mediterranean climatic category as the replacement. But we declare that this would never change all valuable findings obtained in the present study. Figure 1 demonstrates the locations of the 11 stations, whereas the general geographical and climatological features about each of them are shown in Table I. Availabilities of the SPEI had been verified by original authors for the selected stations (Vicente-Serrano *et al.*, 2010a) and globally (Vicente-Serrano *et al.*, 2010b). The SC-PDSI devised by Wells *et al.* (2004) was also calculated for comparing the capability of different indices in this study. Time series of monthly total precipitation and monthly average temperature were downloaded from the Global Historical Climatology Network-Monthly database (available on line at <http://www.ncdc.noaa.gov/ghcnm/>). The precipitation and temperature, respectively, from Global Historical Climatology Network-Monthly versions 2 and 3 were all continuous data and previously checked by means of a quality control process adjusted anomalous records. Datasets used for drought analysis span from 1900 to 2012, more than 100 years and are ideal for statistical treatments. Besides, soil available water (holding) capacity needed to derive the SC-PDSI at each site was obtained from a globally gridded digital format dataset of available water capacity (with a $1^\circ \times 1^\circ$ spatial resolution) provided by Webb *et al.* (2000).

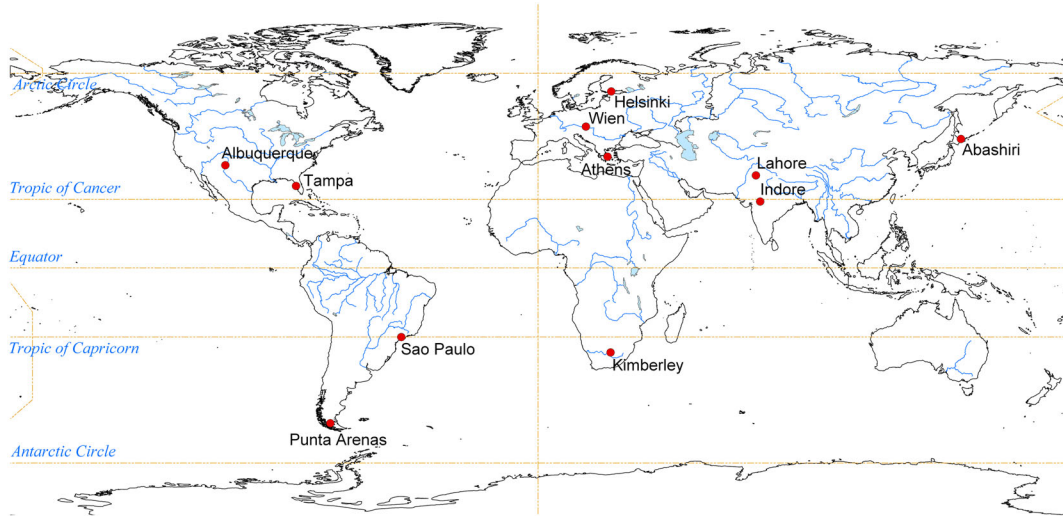


Figure 1. Location of the selected stations from different climate divisions

Table I. Geographical and climatological features of the selected stations

Station	Location	Elevation (m)	P (mm) ^a	T (°C) ^a	Climate category
Lahore	31°36'N, 74°18'E	214	543.8	24.5	Subtropical continental
Sao Paulo	23°36'S, 46°54'W	795	1450.9	18.8	Tropical humid
Athens	38°00'N, 23°42'E	107	396.5	18.0	Mediterranean
Abashiri	44°00'N, 144°18'E	39	830.6	6.1	Temperate oceanic
Kimberley	28°48'S, 24°46'E	1250	419.4	18.1	Subtropical savanna
Indore	22°42'N, 75°48'E	567	948.5	24.8	Tropical monsoon
Helsinki	60°18'N, 25°00'E	53	663.1	5.0	Transitional humid
Albuquerque	35°06'N, 106°36'W	1620	217.6	13.5	Temperate semi-arid
Punta Arenas	53°00'S, 70°54'W	37	414.0	6.3	Temperate cold
Tampa	28°00'N, 82°30'W	3	1210.0	22.5	Subtropical humid
Wien	48°18'N, 16°24'E	212	659.4	9.8	Temperate continental

P , annual total precipitation; T , annual-mean temperature.

^a Both are estimated using the observational datasets of 1900–2012.

Concepts of water balance adopted by the SPEI and PDSI

In fact, the SPEI is analogous and is based on the calculation procedure of SPI. Instead of solely using monthly precipitation as its input data (as the SPI does), the SPEI uses monthly difference between precipitation and PET, which stands for a simple climatic water balance (Thornthwaite, 1948).

$$d_i = P_i - \text{PET}_i \quad (1)$$

where i denotes the i th month in the monthly time series, and this provides a simple measure of water surplus or deficit for the analysed month. Then, the calculated d_i values can be aggregated at different temporal scales (e.g. 12 months) to obtain corresponding accumulated water difference $d_{i,j}^k$ in a given month j of year i , which is depended on the chosen time scale k and calculated using

$$d_{i,j}^k = \sum_{l=13-k+j}^{12} d_{i-1,l} + \sum_{l=1}^j d_{i,l} \text{ for } j < k \quad (2a)$$

and

$$d_{i,j}^k = \sum_{l=j-k+1}^j d_{i,l} \text{ for } j \geq k \quad (2b)$$

where $d_{i-1,l}$ and $d_{i,l}$ are monthly $P - \text{PET}$ in the month l of years $i - 1$ and i , respectively, derived by Equation (1); and calculation of the PET was conducted following the Thornthwaite's method. With accumulated difference series for $d = P - \text{PET}$, the SPEI time series at different temporal scales could then be calculated using the LLG distribution as their theoretical frequency distribution function and classical approximation of standardization (refer to Vicente-Serrano *et al.*, 2010a).

Opposite to the actual (observational) precipitation, the PDSI defined a climatically appropriate for existing conditions (CAFEC) precipitation, i.e. the minimum amount of precipitation needed to maintain a normal soil moisture level for a certain region. This site-dependent CAFEC precipitation for a single month can be found as

$$\tilde{P} = \alpha_i \text{PET} + \beta_i \text{PR} + \gamma_i \text{PRO} + \delta_i \text{PL} \quad (3)$$

where $i = 1, 2, \dots, 12$ is the i th month in a calendar year, α , β , γ and δ are weighting factors (called water-balance coefficients) for a particular location and estimated in the following way:

$$\alpha_i = \frac{\overline{\text{ET}_i}}{\overline{\text{PET}_i}}, \beta_i = \frac{\overline{\text{R}_i}}{\overline{\text{PR}_i}}, \gamma_i = \frac{\overline{\text{RO}_i}}{\overline{\text{PRO}_i}} \text{ and } \delta_i = \frac{\overline{\text{L}_i}}{\overline{\text{PL}_i}} \quad (4)$$

The calculation of α , β , γ and δ involves four values related to soil moisture for each month of every year: evapotranspiration, recharge, run-off and loss (L) along with their complementary potential values: PET, potential recharge, potential run-off and potential loss. These eight components are closely associated with the available water capacity of local soil and actually represent a more complex but comprehensive soil water balance in the surface level. The PDSI utilizes the difference between actual precipitation and computed CAFEC precipitation in a specific month to measure the wet or dry conditions of interest. This water difference named moisture departure is formulated as follows:

$$\tilde{d} = P - \tilde{P} = P - (\alpha_i \text{PET} + \beta_i \text{PR} + \gamma_i \text{PRO} + \delta_i \text{PL}) \quad (5)$$

On the basis of time series of the moisture departure, accurate PDSI/SC-PDSI could then be calculated according to the standard procedures described by Palmer (1965) and Wells *et al.* (2004).

Responses of water surplus/deficit to precipitation and temperature

Performances of monthly time series. Obviously, the SPEI and PDSI models are based on different concepts of water balance and water difference, all taking periodic (e.g. monthly) precipitation and temperature as their input data. Thus, we are interested to explore the relationship between monthly water difference (d for SPEI and \tilde{d} for PDSI as defined by Equations (1) and (5), respectively) and these two meteorological variables first. Figure 2 shows the scatter plots of d versus precipitation (P) and d versus temperature (T) at three given stations. As can be seen, an apparent positive correlation was found between d and P for all the stations, i.e. potential water deficit would fade out quickly and convert to water surplus with

the increase of monthly precipitation. Nevertheless, it should also be noted that the degree of this kind of positive correlation was not the same. For example, the water difference seemed to be excessively dependent on precipitation at Sao Paulo, with a quasi-linear dependence between d and P , whereas the empirical points were found more dispersedly distributed for Albuquerque. And relationship of d and P at Lahore was simply in between. In contrast, evolution of the water surplus/deficit responded differently to temperature variations for these considered stations, as illustrated in the right panes of Figure 2. Significant water shortages formulated and enlarged rapidly as the temperature increased at Lahore (from 0 to nearly -500 mm with temperature increase from 10 to 38°C), and these trends were also easily seen for Albuquerque. With fewer cases of water excess and water deficit rather developed, the assumed water conditions at these two stations were obviously negatively skewed. However, the water difference showed no apparent trend with fluctuations of the temperature at Sao Paulo, and only slight water deficit was observed because of increases in temperature. Besides, for Lahore, some deflected points representing water surplus or low deficit were also observed because of short-term large water supply by (very) high precipitation during hot periods. Likewise, Figure 3 indicates a similar pattern of dependences between \tilde{d} and P , showing the role of precipitation nearly unchanged in formulation of water surplus/deficit. But the extreme correlation between d and P for Sao Paulo was practically adjusted to make the dependence of water difference on precipitation standardized and that sort of correlations for Albuquerque and Lahore were also intensified. Corresponding water shortages were also decreased as the dependence of water deficit on temperature was greatly reduced and homogenized by the use of \tilde{d} (refer to the right panes of Figure 3), which subsequently cut down the unexpected water demand caused by large PET under high temperatures. So far, a relatively uniform pattern of relationships between monthly water difference and precipitation/temperature was found in Figure 3. The results shown in Figures 2 and 3 are also generally true for all other stations including these three. Therefore, in this perspective, the concept of moisture departure \tilde{d} adopted by the Palmer drought model is preferable and more robust, adjusting and standardizing dependences of monthly water surplus/deficit on both precipitation and temperature.

Some large values were observed in the monthly water difference series (either in terms of d or \tilde{d}), and we also compared them with their local annual average precipitation (as reported in Table I). The boxplot, Figure 4, presents percentages of maximum monthly water surplus/deficit with respect to individual annual precipitation for

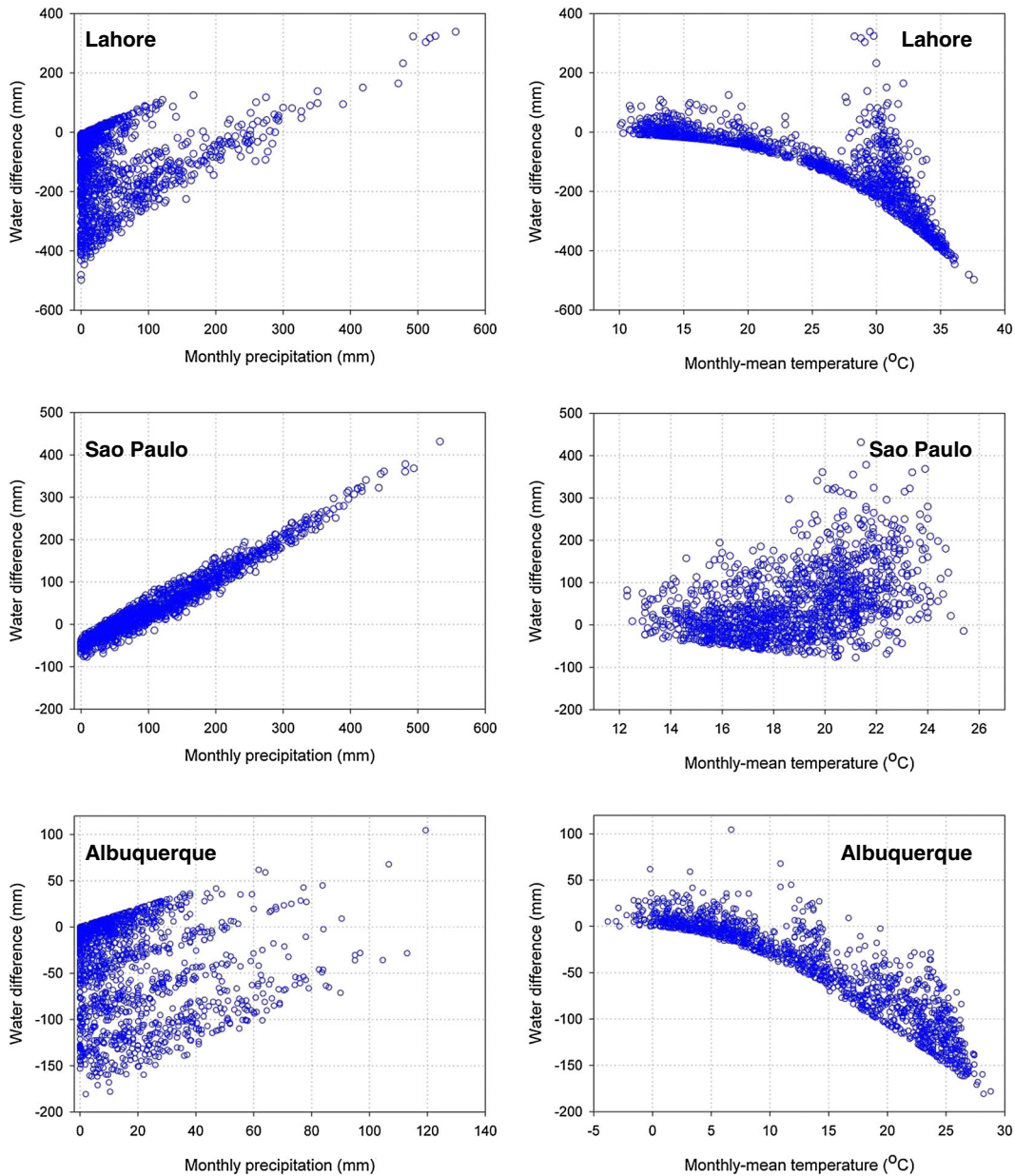


Figure 2. Scatter plots of monthly water difference d versus precipitation (left) and temperature (right) at Lahore, Sao Paulo and Albuquerque

the 11 stations. In cases of water surplus, as can be seen, the range of these maximum differences among the stations was high, on matter using d or \tilde{d} . Although the latter \tilde{d} showed a slightly larger variation than d for different stations, they too collectively displayed almost equal mean values, i.e. the average of maximum monthly water surplus approximately accounted for 43% of annual total precipitation. This noticeable uncertainty is largely attributed to the high spatial variability of precipitation (which is certainly the most important water source for any place at any time) and therefore is well acceptable. But for water deficit that is of more significance to the occurrence of droughts, the maximum monthly water

deficit in terms of d presented an even higher variability among all stations, ranging from 5% to 92% of annual total precipitation. This extremely high spatial variability could introduce substantial unreliability in the water deficit series derived by d . For example, an assumed water deficit as large as 90% of local annual precipitation in just a single month is logically incredible and meaningless. On the contrary, the use of the \tilde{d} depicted a different monthly water deficit series having a fairly low spatial variability among the selected stations, and the average of maximum monthly water deficit was around 18% relative to annual total precipitation. This implies the possibility that an appropriate and stable ratio of

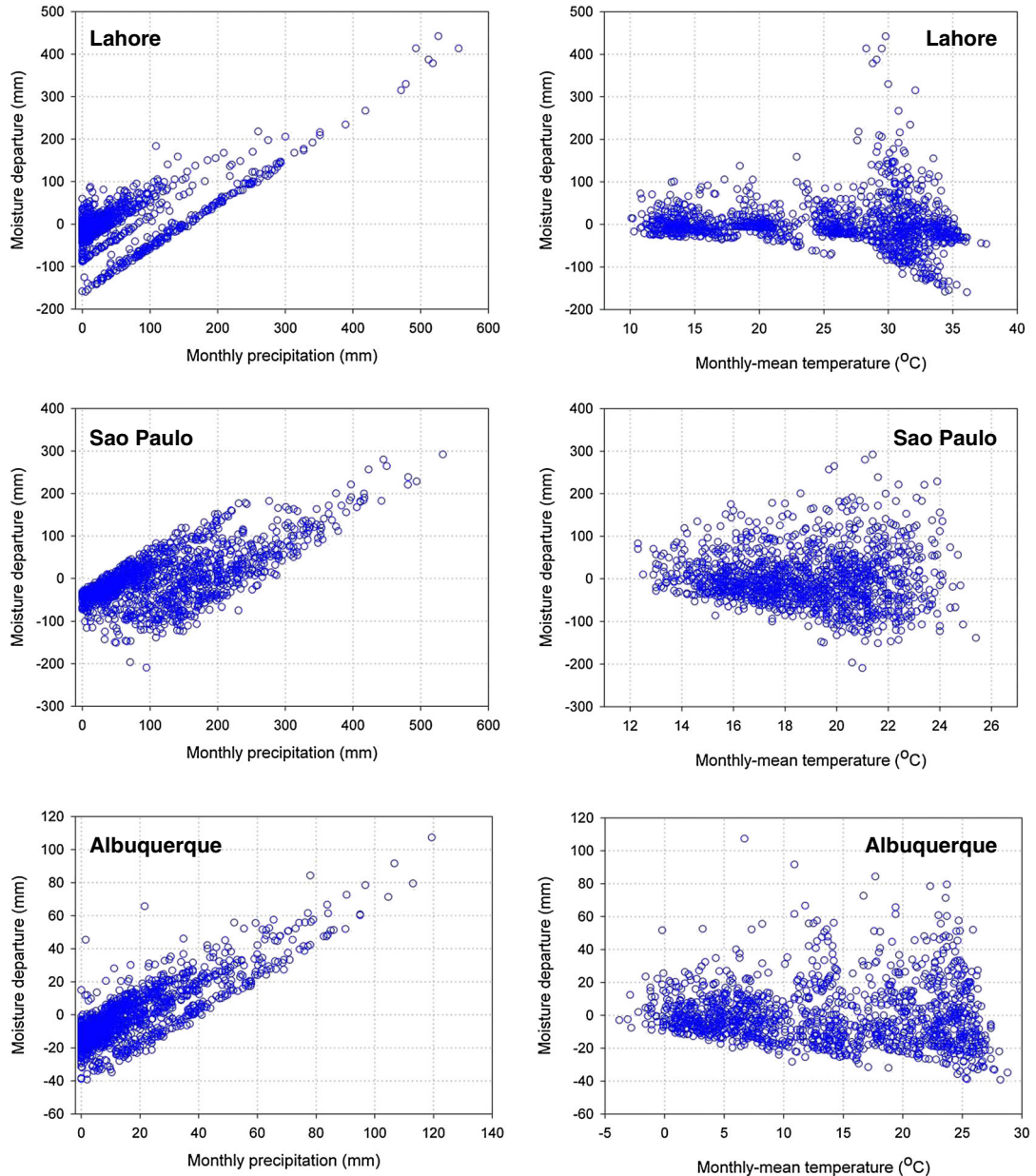


Figure 3. Scatter plots of monthly moisture departure \tilde{d} versus precipitation (left) and temperature (right) at Lahore, Sao Paulo and Albuquerque

maximum monthly water deficit to annual precipitation exists for different climatological regions or globally.

Accumulated cases for multiple temporal scales. We also considered the dependence of accumulated water difference on corresponding precipitation and temperature. For this purpose, the monthly water differences derived by Equations (1) and (5) were separately aggregated at multiple temporal scales of 1, 3, 6, 9, 12, 18, 24, 36 and 48 months using Equation (2); the original monthly precipitation was summed, and the monthly mean temperature was averaged in a sliding manner accordingly. Pearson's classical correlation coefficient r

was used to investigate the proposed relationships here. It is no surprise that Figures 5 and 6 provide completely different results. As can be seen from Figure 5, the positive correlation between accumulated d values and summed precipitation varied a lot among different stations and temporal scales, and high correlations were observed mainly for 12, 24, 36 and 48 monthly time series. However, there were also exceptions such as the Sao Paulo and Indore stations, whose accumulated d values were highly correlated with summed precipitation at all the time scales of analysis. As for the relationship between accumulated d values and averaged temperature, apparent negative correlations were found for all the

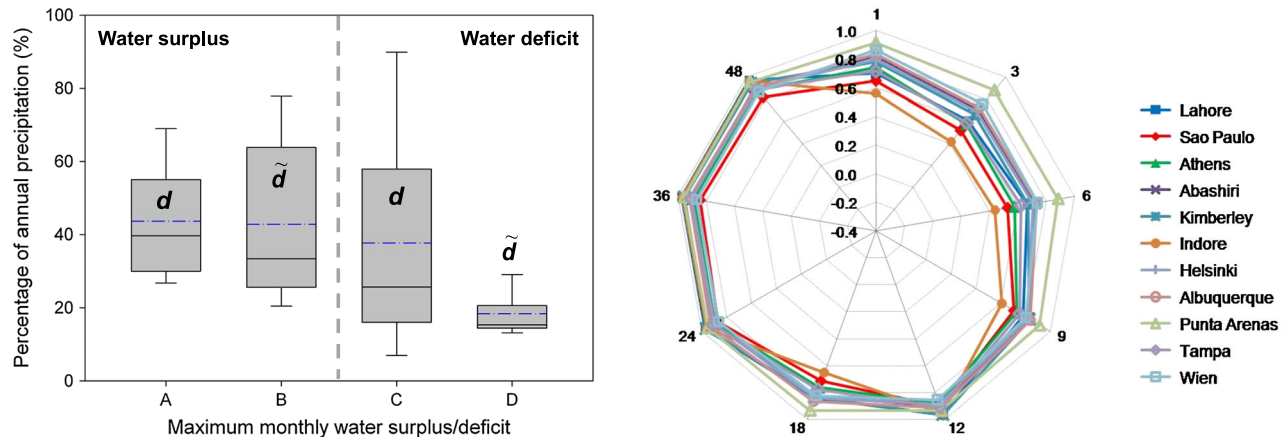


Figure 4. Percentage of maximum monthly water surplus/deficit with respect to annual precipitation for all the selected stations

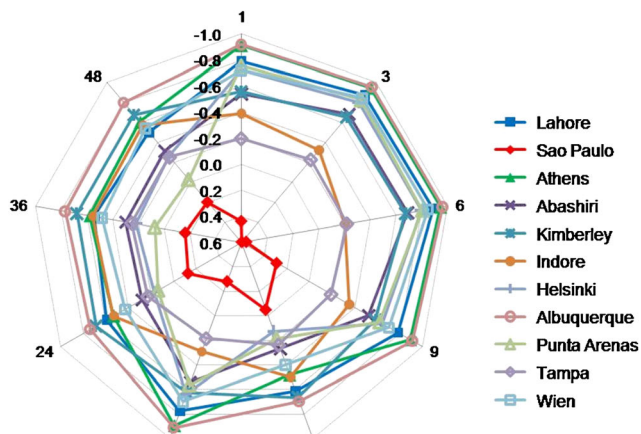
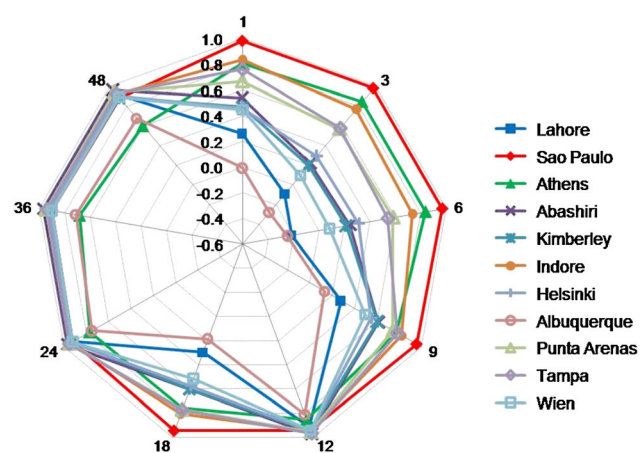


Figure 5. Pearson correlation of accumulated water difference d versus summed precipitation (up) and averaged temperature (down) at various temporal scales for all the selected stations

examined stations except for Sao Paulo. But again, no similar trends existed for each of them, particularly at the temporal scales of 9–24 months. In addition, the notable

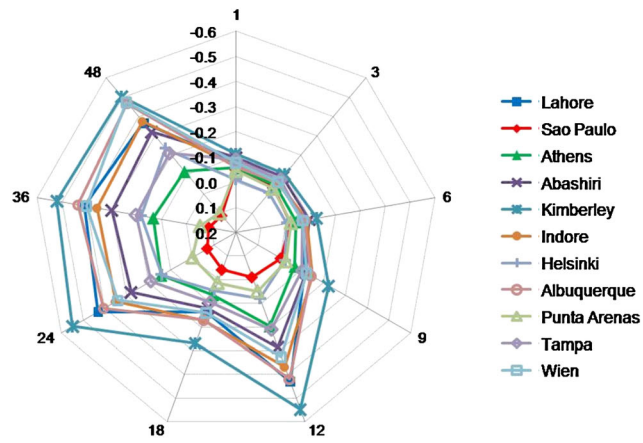


Figure 6. Pearson correlation of accumulated moisture departure \tilde{d} versus summed precipitation (up) and averaged temperature (down) at various temporal scales for all the selected stations

positive dependences of accumulated d values on temperature for Sao Paulo (especially at the shortest time scales, e.g. 1, 3 and 6 months) were rather incredible and unreasonable. Overall, in terms of d for accumulated periods, precipitation and temperature would contribute near equally to the formulation of water surplus/deficit.

On the contrary, Figure 6 presents a more uniform pattern of correlation for the accumulated \tilde{d} values, both with summed precipitation and averaged temperature. Specifically, a high positive correlation ($r > 0.8$) was found between accumulated \tilde{d} values and precipitation at time scales of 12, 24, 36 and 48 months, whereas the correlations at all other temporal scales were slightly lower (r ranging from 0.5 to 0.8). Similarly, the negative correlation coefficients between accumulated \tilde{d} values and temperature were all below -0.6 , achieving larger values at 12, 24, 36 and 48 months time scales too; and the correlations for other temporal scales (e.g. 1, 3, 6, 9 and 18 months) were relatively low. Although positive correlations were still presented for Sao Paulo at long-term time

scales (more than 18 months), this was actually very rare, and all the correlations were not significant ($r < 0.1$). Contrasting to the d values, accumulated water surplus/deficit represented by \tilde{d} responded consistently to precipitation and temperature for different stations and temporal scales in general. And the role of precipitation was apparently over that of temperature in forming regional water anomalies, which suits our intuitive feelings and prior knowledge well.

Summary

It is clear that the water difference d used by SPEI responded differently to variations of precipitation and temperature for different climatic conditions, both at monthly and seasonal temporal scales. The monthly d series was found excessively depended on temperature data, yielding significantly increasing water deficit with increase of PET under high temperatures. However, the abnormally large water deficit due to large PET can be unreliable as actual evapotranspiration tends to be far less than the PET for low precipitation but very high temperature in dry seasons, like what might have happened in places already prone to drought (e.g. Lahore and Albuquerque). This was confirmed by the maximum monthly water deficit reported by d values, which constituted a large part of local annual precipitation, and this proportion showed very high spatial variability among different stations. But the maximum water deficit expressed by \tilde{d} values showed a low-variably fixed proportion comparing with the annual total precipitation for all the analysed stations.

In short, the varying relationship between water difference d and precipitation/temperature could undermine the declared spatial consistency and comparability of the SPEI, subsequently reducing its effectiveness in practical use. But fortunately, the moisture departure \tilde{d} defined by the PDSI, by comparison, can adjust and homogenize the dependence of water conditions on temperature while retaining the role of precipitation and is therefore superior.

METHODOLOGY

In consideration of the desirableness and robustness of moisture departure \tilde{d} over water difference d , the moisture deficit/surplus time series are suggested to be obtained by aggregation for a range of accumulated periods (1–48 months) using Equations (2)–(5) to derive the newly proposed SPDI through subsequent probabilistic analyses and treatments on moisture departures. And this aims at supporting applicable requirements of multi-scale drought analysis and evaluation for different purposes.

Standardization for obtaining the SPDI series

With the probabilities of \tilde{d} computed by chosen cumulative distribution function $F(x)$, the SPDI can readily be calculated as standardized values of $F(x)$ following the succeeding procedure of approximation standardization after Abramowitz and Stegun (1965), i.e.

$$\text{SPDI} = W - \frac{a_0 + a_1 W + a_2 W^2}{1 + b_1 W + b_2 W^2 + b_3 W^3} \quad (6)$$

where $W = \sqrt{-2 \ln(p)}$ for $p \leq 0.5$, and $p = 1 - F(x)$ is the exceedance probability of a certain \tilde{d} value. For $p > 0.5$, p should then be replaced by $1 - p$, and the sign of the computed SPDI is also reversed. The needed constants for calculation are given as follows: $a_0 = 2.515517$, $a_1 = 0.802853$, $a_2 = 0.010328$, $b_1 = 1.432788$, $b_2 = 0.189269$ and $b_3 = 0.001308$. After this process of standardization, the SPDI becomes a standardized variable (approximately following a standardized normal distribution with zero mean and unit standard deviation) and shares the same quantiles/probabilities for classifying droughts as used by the SPI and SPEI. It is easy to see that a particular SPDI value is consistent and stands for the same water condition at different times and locations, and it can therefore be compared with other SPDI values over time and space.

Selection of a suitable probability distribution

The \tilde{d} time series aggregated at different temporal scale are assumed to be independent random variables, and this is quite feasible in practice. Thus, for calculation of SPDI, an appropriate probability distribution that can well model the frequency of the \tilde{d} values accumulated at different periods is needed. We focused and tested four 3-parameter candidate distributions, i.e. LLG, generalized extreme value (GEV), Pearson type III and log-normal, because none of them could be rejected for the \tilde{d} series of different temporal scales at a 0.05 significance level according to the Kolmogorov-Smirnov and Anderson-Darling tests. And in most cases, the empirical frequency histogram of the \tilde{d} series could be satisfactorily represented by all the theoretical curves of these four selected distributions, and their similarities in fitting capacity indicate the use of any one of them showing no apparent superiority.

Visual inspection using L-moment ratio diagrams. As a useful visual inspection tool, L-moment ratio diagrams can be used to select the most suitable distribution because they allow for comparison of shape characteristics (i.e. L-moments that specify a unique distribution, especially the L-skewness τ_3 and L-kurtosis τ_4) for empirical distribution of the \tilde{d} series calculated at various temporal scales with theoretical distributions (Hosking,

1990; Vogel and Fennessey, 1993). Figure 7 shows the L-moment ratio diagrams for \tilde{d} series accumulated at short-term (3 months), medium-term (18 months) and long-term (36 months) temporal scales for all the 11 stations. It is evident that among the four candidates, the GEV, Pearson III (PE3) and log-normal distributions collectively produced a satisfactory fit to the empirical frequency of the \tilde{d} series at all analysed timescales as the

sample L-statistics oscillated around their theoretical curves, whereas LLG distribution actually attracted the least empirical points at any accumulated durations. However, there were also outliers indicating the difficulty for finding optimal probability distribution of the \tilde{d} series at some stations, e.g. 18 and 36 months for Wien and 36 months for Abashiri. Other two-parameter and three-parameter distributions (e.g. normal, exponential, Gumbel

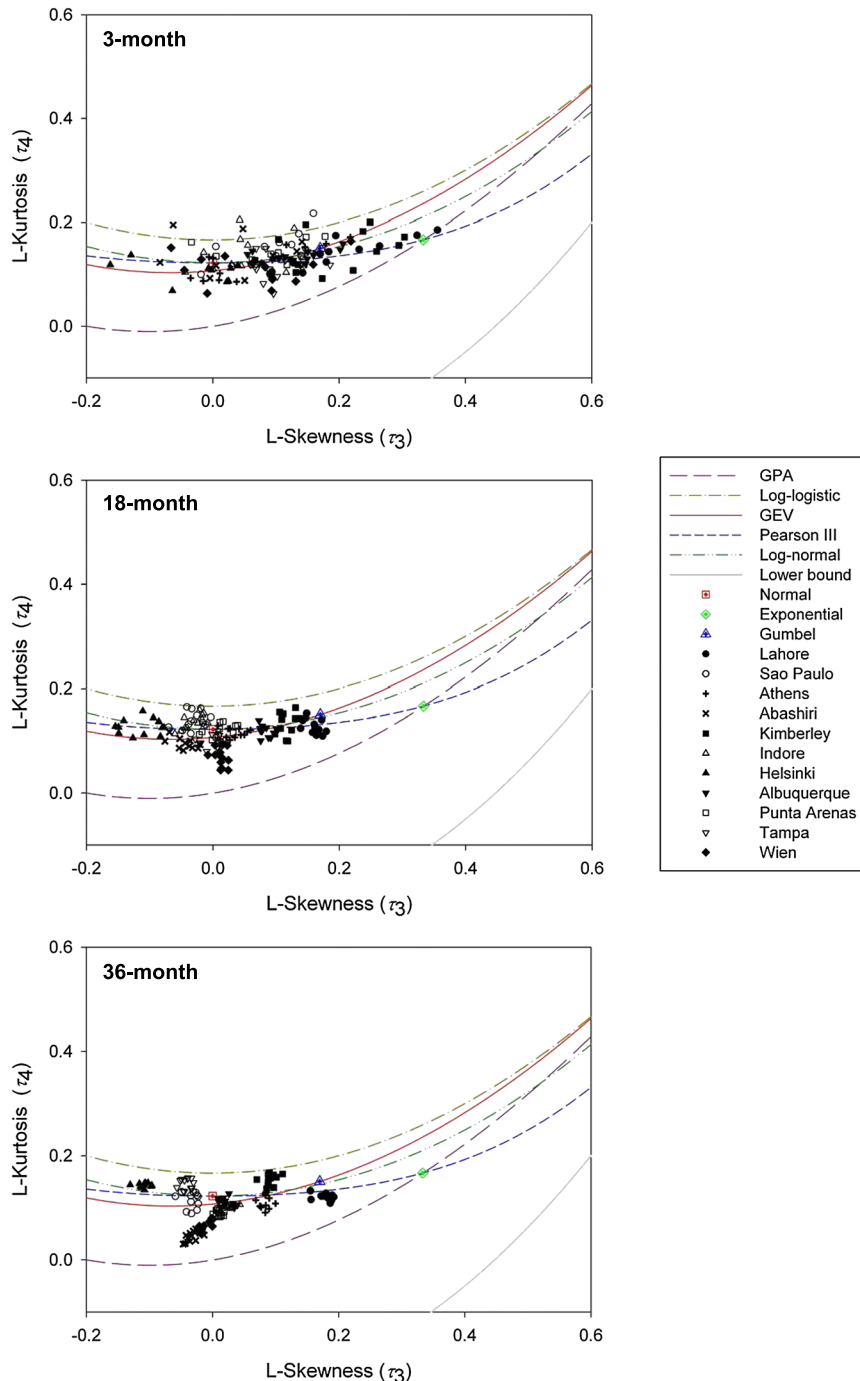


Figure 7. L-moment ratio diagrams of \tilde{d} series calculated at time scales of 3, 18 and 36 months for all the selected stations

Table II. Average fitting biases of \tilde{d} series of various temporal scales for 11 selected stations using four theoretical distributions

Criterion	Distribution	Time scale (month)						Average	
		1	3	6	9	12	18	24	
BIAS ^a	Generalized extreme value	0.0036	0.0029	0.0030	0.0032	0.0033	0.0031	0.0034	0.0033
	Log-logistic	0.0053	0.0040	0.0034	0.0032	0.0030	0.0031	0.0032	0.0036
	Log-normal	0.0028	0.0025	0.0026	0.0028	0.0027	0.0027	0.0029	0.0027
	Pearson III	0.0032	0.0023	0.0026	0.0027	0.0027	0.0027	0.0029	0.0027
	Generalized extreme value	0.0226	0.0198	0.0197	0.0205	0.0206	0.0193	0.0189	0.0192
	Log-logistic	0.0255	0.0236	0.0232	0.0250	0.0254	0.0243	0.0239	0.0251
	Log-normal	0.0218	0.0194	0.0194	0.0204	0.0207	0.0193	0.0188	0.0196
	Pearson III	0.0224	0.0194	0.0195	0.0203	0.0206	0.0192	0.0188	0.0212
	Generalized extreme value	-863.1	-888.6	-886.4	-876.7	-872.9	-884.2	-881.5	-867.2
Akaike information criteria	Log-logistic	-834.3	-847.5	-848.9	-830.0	-825.1	-832.4	-831.2	-815.8
	Log-normal	-869.8	-892.9	-889.2	-876.7	-872.0	-884.8	-882.5	-865.7
	Pearson III	-864.6	-893.0	-889.3	-878.1	-872.3	-885.6	-882.6	-864.9

^aThe absolute values of abs(BIAS) are shown here.

and generalized Pareto) reflected in the L-moment ratio diagrams showed little competitiveness altogether.

Fitting biases by goodness-of-fit statistics. Goodness-of-fit statistics are also most popularly used for statistical model selection, such as bias (BIAS), root mean square error (RMSE) and Akaike information criteria (AIC). Their expressions and applying details used here are the same as those recommended by Zhang (2005). In the case of BIAS, RMSE and AIC, the smaller they are, the better fit the model provides. Thus, the results revealed by visual inspection of L-moment ratio diagrams for the d series were also confirmed by computed BIAS, RMSE and AIC values shown in Table II, because the GEV, log-normal and PE3 distributions resulted similarly small fitting biases on the whole (averaged by all the stations for each time scale). Again, the LLG distribution produced relatively larger goodness-of-fit statistics, especially in terms of the AIC and RMSE values.

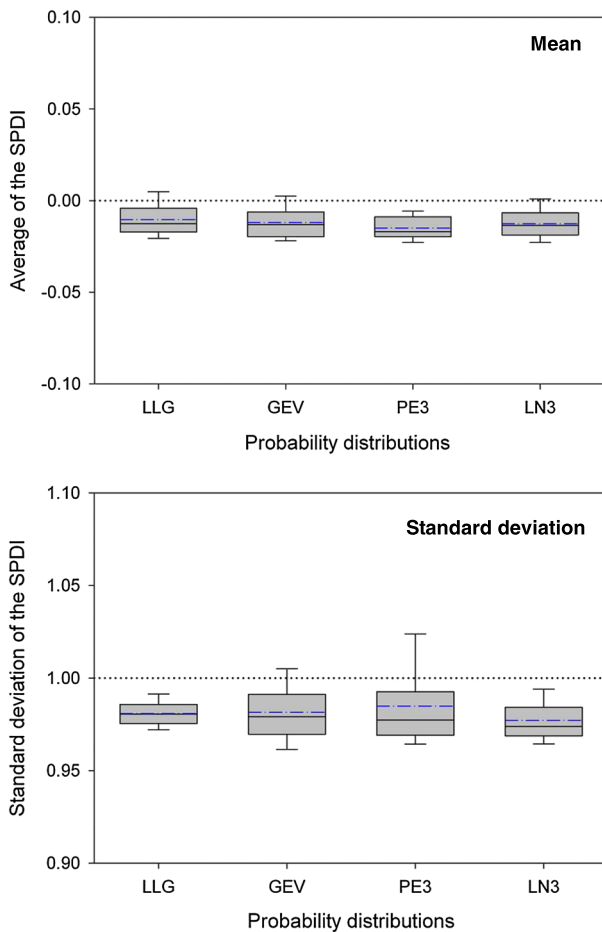


Figure 8. Mean and standard deviation values of the calculated SPDIs at various temporal scales (1–48 months) using the four theoretical distributions for all the selected stations

Statistical properties of computed SPDI series. Because there was no sufficient evidence to determine the use of which probability distribution (e.g. GEV, PE3 or log-normal) to model empirical frequency of the \tilde{d} series, we made an additional comparison on the basis of expected statistical properties of the SPDIs calculated by different distributions (Vicente-Serrano *et al.*, 2012). As has been noted earlier, the SPDI is approximately a standardized variable, whose long-term average and standard deviation are expected to equal zero and one, respectively. Figure 8 shows two boxplots of mean and standard deviation of the SPDI series computed at various temporal scales (1–48 months) using the four theoretical distributions for all the stations. As can be seen, the SPDI derived from some distributions was deficient in comparison to expected average and standard deviation values. For example, the mean of averaged SPDIs was negatively deviated for PE3 distribution, whereas the mean of the averages was close to zero for LLG and GEV distributions. However, low variability of the average values among different stations indicates the possibility of adopting specific candidate distribution (at least one of the four) to establish reliable spatial comparisons because a particular value of SPDI would represent roughly same water condition in all cases. The standard deviation of the

SPDI series also differed from each other for the four distributions. The LLG and log-normal (LN3) distributions produced standard deviation values markedly smaller than one, which implies against use of them for calculation of the SPDI. It is delightful to see that GEV and PE3 distributions resulted in standard deviations around one, whereas the latter had slightly larger spatial variability.

Statistical comparisons of expected frequency of specific SPDI value relating to given occurrence possibility were also conducted here. According to the law of standard normal distribution, one value is expected to be less than -1.65 or greater than 1.65 with the same cumulative probability of 0.05, whereas exceeding -2.33 or 2.33 similarly corresponds to a probability of 0.01. Considering the monthly SPDI series starts from the year of 1904 for the longest 48-month time scale, and the length of the total time series turns out to be 1308 months (109 years of 1904–2012). Therefore, on average, about 65.4 events of the SPDI values above 1.65 (or below -1.65) and 13.08 events of the SPDI values above 2.33 (or below -2.33) would be expected altogether. Figure 9 compares the observed (boxplots) and expected (dotted lines) frequency of the SPDI values exceeding these four thresholds. On the basis of various temporal scales

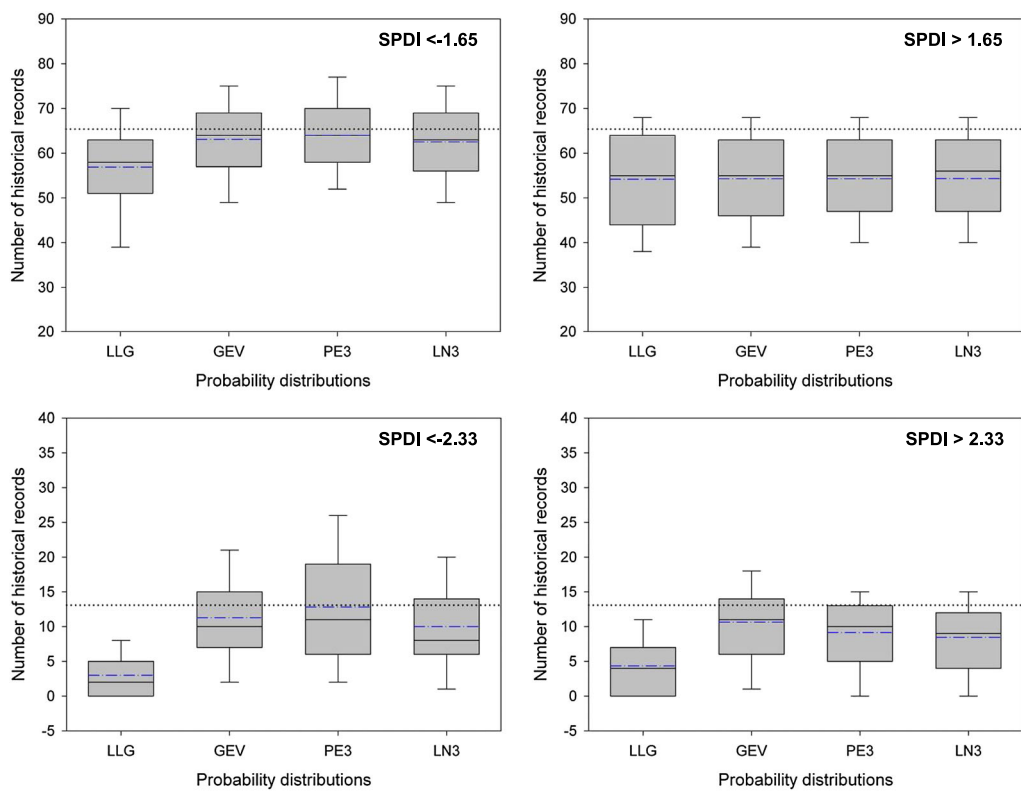


Figure 9. Frequency of low (less than -1.65 or -2.33) and high values (greater than 1.65 or 2.33) of the calculated SPDI series at various temporal scales (1–48 months) using the four theoretical distributions for all the selected stations

(1–48 months) for all the stations, it was found that the frequency of computed SPDI values exceeding ± 1.65 generally followed the expected frequency for all the four distributions used for calculation. Although all the examined distributions tend to systematically underestimate the frequency of $SPDI > 1.65$ (wet condition), this would actually not affect the assessment of the occurrence of corresponding drought events. In contrast, the LLG distribution substantially undervalued and failed to detect the frequency of SPDI values exceeding ± 2.33 , whereas all other three distributions provided better and acceptable results. But in terms of closeness to expected values and spatial variability among different stations, the GEV and PE3 distributions also seemed superior to log-normal distribution.

In spite of the similarity between PE3 and GEV distributions, we found additional poor behaviours of PE3 distribution at the most extreme cases. For example, with

very low \tilde{d} values, the PE3 distribution could derive extremely low cumulative probabilities, and even many zeros were also observed, which would cause difficulty and impracticability in subsequent standardized transformation to obtain SPDI values. The aforementioned findings suggest the use of a GEV distribution as the optimal probability distribution for \tilde{d} series to calculate SPDI.

The GEV distribution and parameters estimation. Using the GEV distribution, cumulative distribution function of the d series is given by

$$F(x) = \exp\left\{-\left[1 - \kappa\left(\frac{x - \mu}{\alpha}\right)\right]^{\frac{1}{\kappa}}\right\} \quad (7)$$

where μ , α and κ are location, scale and shape parameters, respectively. These parameters can be

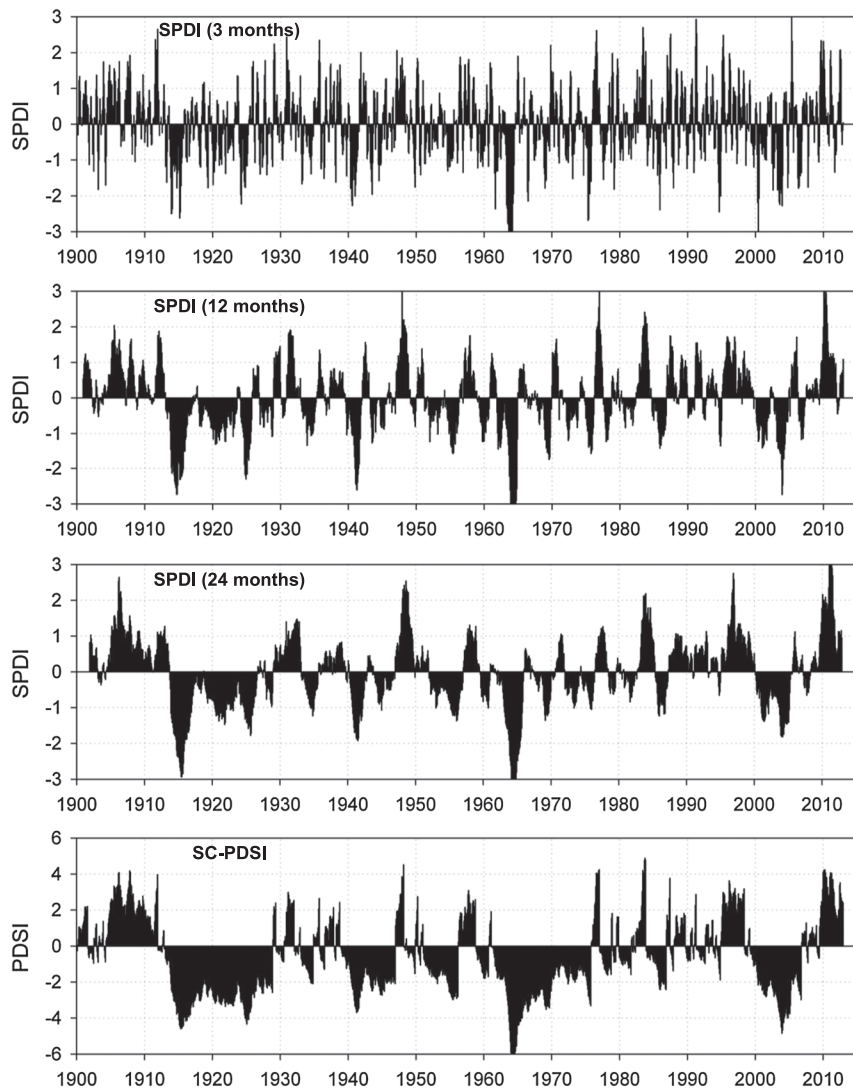


Figure 10. Evolution of 3, 12 and 24 months SPDI and the SC-PDSI series at Sao Paulo station during the period of 1900–2012

estimated following the L-moments approach described by Hosking (1990), e.g.

$$\hat{\kappa} = 7.8590z + 2.9554z^2 \quad (8a)$$

$$\hat{\alpha} = \frac{\lambda_2 \hat{\kappa}}{\Gamma(1 + \hat{\kappa})(1 - 2^{-\hat{\kappa}})} \quad (8b)$$

$$\hat{\mu} = \lambda_1 + \frac{\hat{\alpha}}{\hat{\kappa}} [\Gamma(1 + \hat{\kappa}) - 1] \quad (8c)$$

where $z = 2/(3 + \tau_3) - 0.6309$; $\tau_3 = \lambda_3/\lambda_2$ is the L-skewness; and λ_1 , λ_2 and λ_3 are the first three L-moments of the sample series, obtained from linear combinations of the probability weighted moments using formulas

$$\lambda_1 = \beta_0 \quad (9a)$$

$$\lambda_2 = \beta_0 - 2\beta_1 \quad (9b)$$

$$\lambda_3 = \beta_0 - 6\beta_1 + 6\beta_2 \quad (9c)$$

where β_0 , β_1 and β_2 are the first three-order probability weighted moments of the sample and are computed with the unbiased estimators (Vogel and Fennessey, 1993).

$$\beta_0 = \frac{1}{n} \sum_{j=1}^n x_j \quad (14a)$$

$$\beta_1 = \sum_{j=1}^{n-1} \left[\frac{(n-j)}{n(n-1)} \right] x_{(j)} \quad (10b)$$

$$\beta_2 = \sum_{j=1}^{n-2} \left[\frac{(n-j)(n-j-1)}{n(n-1)(n-2)} \right] x_{(j)} \quad (10c)$$

here, $x_{(j)}$ represents the ordered values of a sample of size n with $x_{(1)}$ being the largest observation and $x_{(n)}$ the smallest, i.e. $x_{(1)} \geq \dots \geq x_{(j)} \geq \dots \geq x_{(n)}$.

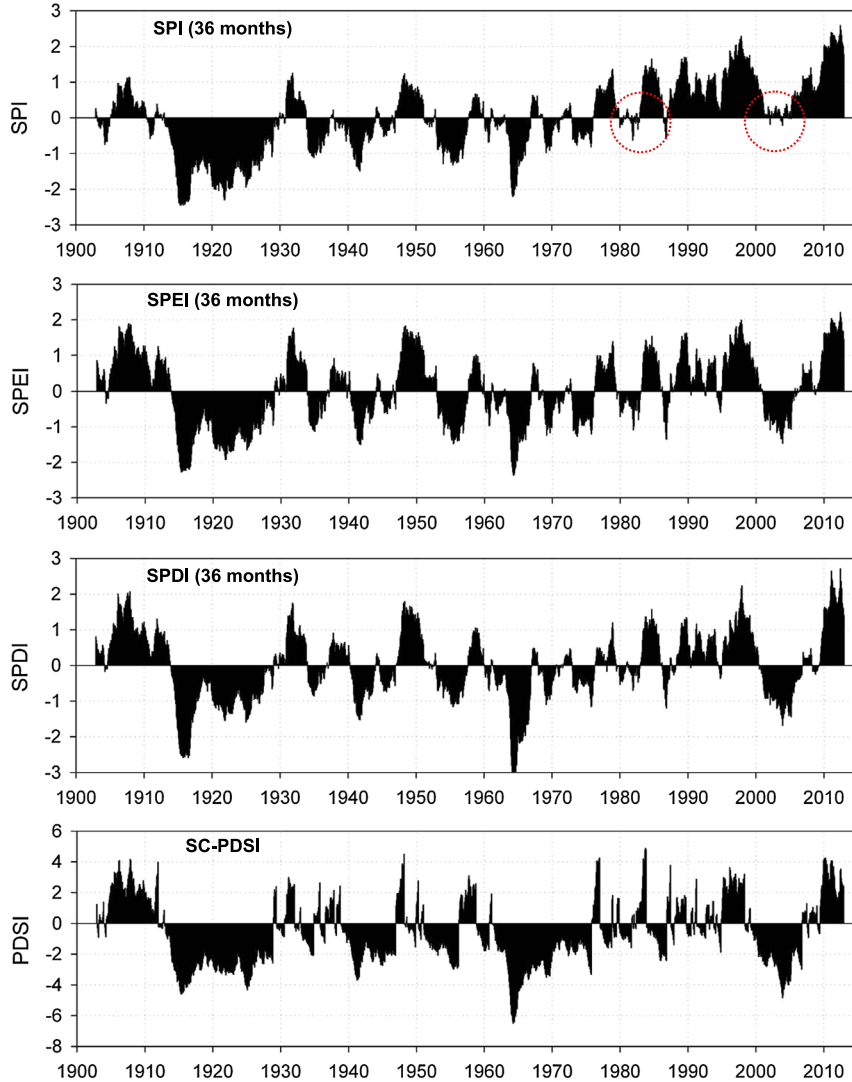


Figure 11. Evolution of 36 months SPI, SPEI and SPDI and SC-PDSI series at Sao Paulo station during the period of 1900–2012

RESULTS

Comparisons of historical records by multiple drought indices

Following the aforementioned proposed methodology, the monthly time series of the SPDI with nine accumulation periods (1, 3, 6, 9, 12, 18, 24, 36 and 48 months) was calculated for all the selected stations between 1900 and 2012. For comparisons of multiple drought indices, corresponding SPI, SPEI and SC-PDSI records were also reconstructed. The results show that the evolution of these drought indices displayed high agreements for most of the stations and time scales. For example, Figure 10 compares the 3, 12 and 24 months SPDI and the SC-PDSI series at Sao Paulo station through the periods of 1900–2012. It was found that the main and most severe drought episodes occurred in the decades of 1910–1920, 1940, 1950, 1960–1970 and 2000 were clearly identified by the SC-PDSI as well as SPDI calculated at multiple temporal scales. Nevertheless, unlike the SC-PDSI (which generally presented only a few of prolonged wet and dry spells), the multi-scalar SPDI seemed to be more sensitive to the changes in the condition of water demand and supply and showed significant fluctuations in general (e.g. for time scales of 3 and 12 months), indicating occurrences of more drought events with different duration and severity. Because these multivariate drought characteristics are of great significance in drought analyses and design, we would like to conclude that the SPDI with multiple detecting time windows has advantages over SC-PDSI and is more flexible and operable in practical drought monitoring and assessment.

However, several meteorological stations such as Sao Paulo has experienced marked increases in temperature over the past more than 100 years, e.g. Sao Paulo (0.28 °C per decade), Albuquerque (0.16 °C per decade) and Wien (0.14 °C per decade). We are wondering whether the high agreements among different indices in announcing droughts would be retained when being exposed to such high changes in local temperature. To this end, Figure 11 shows the evolution of 36 months SPI, SPEI and SPDI and the SC-PDSI for Sao Paulo between 1900 and 2012 in which the main long-term drought episodes before 1980 were all captured by the four indices. But in comparison to SPEI, SPDI and SC-PDSI, the moderate drought intervals during the 1980s began to disappear, whereas the severer droughts happened in the first decade of the 21st century were completely neglected by SPI in the end. As such, the SPI failed to recognize all the historical drought periods under changing climate conditions due to its only accounting for precipitation variation. In contrast, the SPDI together with SPEI and SC-PDSI was competent for drought detection with increased

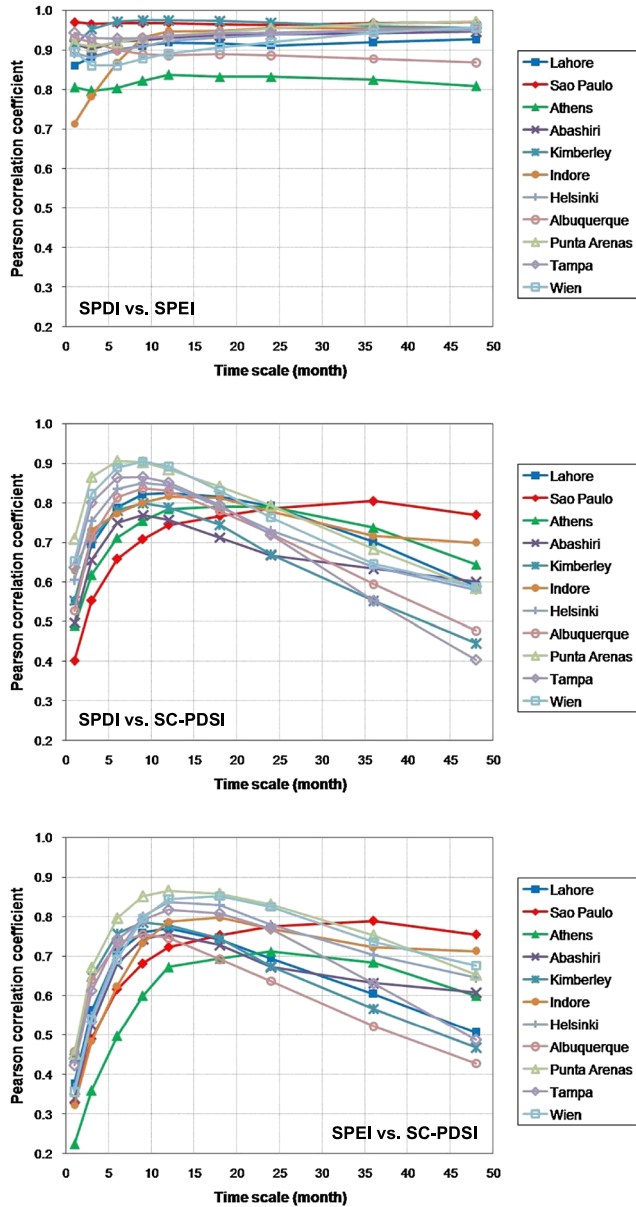


Figure 12. Pearson correlation among time series of the SPDI and SPEI calculated at various temporal scales and the SC-PDSI for all the selected stations

temperature because they could consider the additionally higher water demand by increase in PET. Therefore, high agreements among the SPDI, SPEI and SC-PDSI could be found for all other stations at certain temporal scales. Figure 12 reports the correlations among the 1900–2012 series of 1–48 months SPDI and SPEI and the SC-PDSI for each of the stations. As it is shown, correlations between the SPDI and SPEI were very high for the different series of all analysed time scales, with nearly all minimum Pearson correlation coefficients greater than 0.8. There were also strong correlations between the SPDI and SC-PDSI, and their maximums spanned between 0.77

and 0.91 for temporal scales of 1–48 months, though the correlations peaking at different accumulated periods (e.g. 9–12 months for most of the stations but 6, 24 and 36 months for Punta Arenas, Athens and Sao Paulo, respectively). A similar pattern of correlation was also observed between the SPEI and SC-PDSI, but in general, their correlations were relatively low compared with that between the SPDI and either of them. As a result, the newly derived SPDI was highly consistent and correlated with the SPEI and SC-PDSI, with readily higher correlations than that between the SPEI and SC-PDSI.

Evolution of the SPDI under climate change scenarios

Climate change is likely to lead more droughts worldwide both in frequency and magnitude, whereas spatial-temporal variations of precipitation and temperature would also make things even worse. As mentioned earlier, dramatic increases in air temperature have been observed at some stations and places. On the other hand, projections of global future climate indicate that more severe fluctuations and extremes are likely to be seen in precipitation, and its reduction in some continental regions could be up to 20%, which would certainly exacerbate the drought damages (IPCC, 2007). In addition, the impacts of climate change on drought risk will vary over time and space. The SPDI derived in this

study that can be calculated for different temporal scales and spatially comparable is expected to provide explicit drought assessment under changing climate. Thus, for better projection and preparedness with the worst situations, we proposed three hypothetical scenarios for climate sensitivity analysis: progressive increase of 3 °C in temperature, progressive decrease of 20% in precipitation and a combination of these two scenarios during the period of 1900–2012 and investigated the different drought responses to potential climate change impacts using the SPDI.

Figure 13 compares the evolution of the 18 months SPDI under current climatic condition and three climate change scenarios for Sao Paulo, and the differences between the indices of hypothetical scenarios and original data are also shown. With a temporal temperature increase up to 0.28 °C per decade between 1900 and 2012, alternate wet and dry spells were observed at this station under current climate, and the most severe droughts occurred in the decades of 1910–1920, 1940, 1960 and 2000. These main drought episodes were partly duplicated by the SPDI computed for temperature and/or precipitation change scenarios. However, this simple experiment clearly showed an increase in the duration and magnitude of potential drought events at the end of the 20th century and at the beginning of the 21st century,

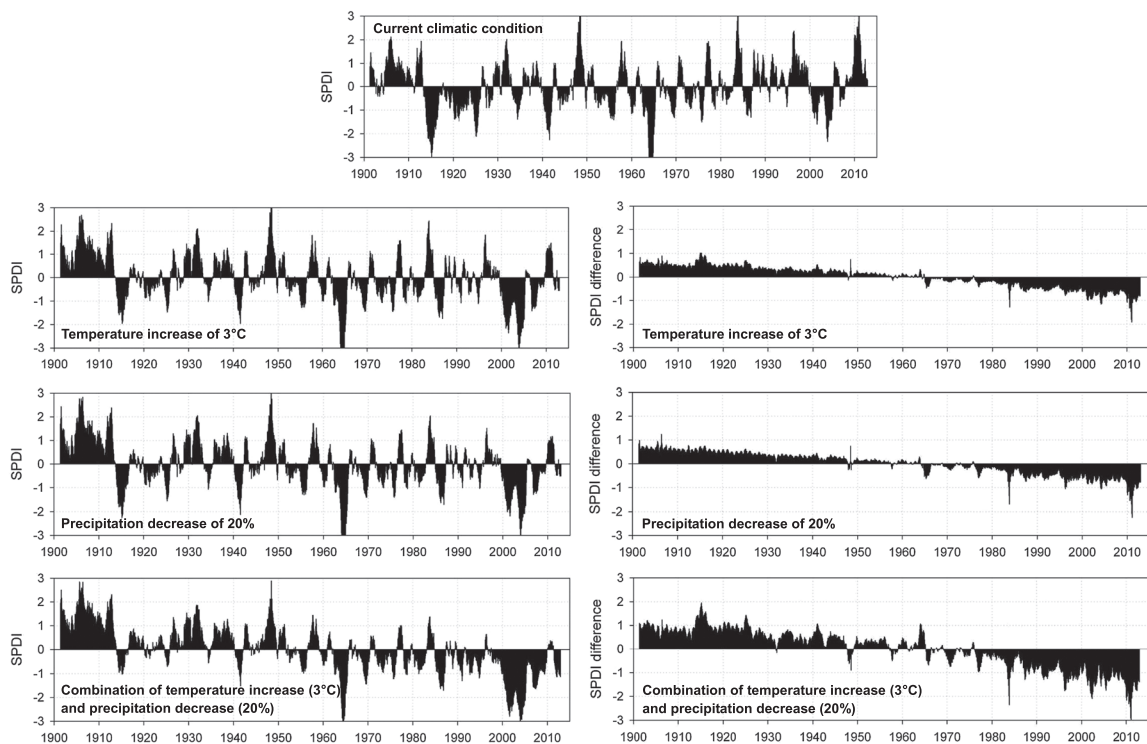


Figure 13. Evolution of 18 months SPDI under current climatic condition and experimental climate change scenarios for Sao Paulo station over the period of 1900–2012 and their differences are also shown

which is directly related to the temperature increase and precipitation reduction. The high agreement between evolutions of the SPDI with temperature increase and precipitation decrease indicates similar impacts of temperature and precipitation changes on future drought risk for this region. On the other hand, because of the increase and decrease in the mean temperature and precipitation series, the new standardized SPDI values indicated less and insignificant drought episodes during the first half of the 20th century while inducing slightly more humid periods (e.g. 1920s and 1930s). All these messages were explicitly reflected by the differences between the computed SPDI series for current and climate change scenarios as well. With the experimental climate change scenarios, more severe drought condition that is likely to be seen at the end of the concerned period is closely associated with specified temporal variations in temperature and precipitation. Furthermore, differences between the SPDI series computed with modelled and real data indicated that water condition at São Paulo would be regularly affected by increases in temperature and decreases in precipitation, i.e. progressively humid and drought episodes are added to the historical records, with the decade of 1960 as their approximate demarcation.

DISCUSSION AND CONCLUSIONS

We identified some problems about the climatic water balance used by SPEI and recommend a more inclusive one, taking into account soil moisture-related hydro-meteorological processes defined by PDSI. That is, by modifying the standardization procedure of PDSI on the basis of the mathematical framework of SPI/SPEI, we made the PDSI in a new multi-scalar drought index, the SPDI. This standardization algorithm (Guttman, 1999) enables an appropriate representation of abnormal wetness and dryness by using the SPDI, which has already been proved by the high agreements and correlations between the SPDI and SPI/SPEI/SC-PDSI. We also assessed the properties and strength of this newly derived drought index in comparison with SPI, SPEI and SC-PDSI for the selected meteorological stations located in different climatologic divisions with diverse local characteristics. Superior to the SPI, the SPDI could recognize the role of temperature increase on drought conditions affected by higher water demand by PET. Meanwhile, adopting stronger concept of physically based water balance in terms of demand and supply, the SPDI standardizes and refines sensitivities of water surplus/deficit to precipitation and temperature variations, resulting potentially preferable and more robust spatial consistency and comparability than SPEI. The main advantages of SPDI over PDSI are its multi-scalar nature

for multi-temporal analyses and the simplicity of calculation, i.e. it escapes the complicated derivation of calibration to obtain site-dependent climatic parameters at a nearly equivalent efficiency in characterizing drought. And experimental performances of the SPDI under proposed temperature and/or precipitation change scenarios indicate its effectiveness in dealing with rising drought problems driven by a climate-changing world.

Some critical conclusions can be drawn as follows: (i) the water difference between precipitation and PET is overly depended on temperature data and responds differently to temperature and precipitation variations for different locations of diverse climatic conditions, which would actually challenge the spatial consistency and comparability of the SPEI, (ii) the physically based water balance and corresponding moisture departure defined by the PDSI are able to regularize the role of precipitation and temperature in analyzing regional water budget for different climates and (iii) the SPDI derived on the basis of probabilistic properties of the moisture departure is also a standardized multi-scalar index that can be calculated at multiple temporal scales of more than 1 month for drought monitoring and management with different purposes, and it combines the simplicity of calculation with sufficient accounting of the physical nature of water supply and demand relating to droughts. The SPI/SPEI is derived solely from the analyses of climate variables such as precipitation and temperature and mainly for consideration of meteorological droughts. In contrast, the PDSI model can provide measurements of some hydrologic variables such as potential surface run-off and soil moisture content, making it meaningful for hydro-meteorological uses. Applications in this study show that all computed SPDI series are highly consistent and correlated with the corresponding SPEIs and SC-PDSIs at the time scales of interest, which suggests that the hybrid SPDI is a competent reference and an alternative to the SPEI and SC-PDSI for future drought analyses, though improvements (e.g. estimation approaches of the PET) are surely welcomed.

ACKNOWLEDGEMENTS

The present work is supported by the Special Basic Research Fund for Methodology in Hydrology by Ministry of Sciences and Technology, China (Grant No. 2011IM011000), the National Key Technology R&D Program by Ministry of Sciences and Technology, China (Grant No. 2013BAC10B02) and the Program of Introducing Talents of Discipline to Universities by Ministry of Education and State Administration of Foreign Experts Affairs, China (the 111 Project, Grant No. B08048).

REFERENCES

- Abramowitz M, Stegun IA. 1965. Handbook of Mathematical Functions, with Formulas, Graphs, and Mathematical Tables. Dover Publications: New York, U.S.; 1046.
- Alley WM. 1984. The Palmer drought severity index: limitations and assumptions. *Journal of Climate and Applied Meteorology* **23**(7): 1100–1109. DOI: 10.1175/1520-0450(1984)023<1100:TPDSIL>2.0.CO;2
- Cook ER, Meko DM, Stahle DW, Cleaveland MK. 1999. Drought reconstructions for the continental United States. *Journal of Climate* **12** (4): 1145–1162. DOI: 10.1175/1520-0442(1999)012<1145:DRFTCU>2.0.CO;2
- Dai A, Trenberth KE, Qian TT. 2004. A global dataset of Palmer drought severity index for 1870–2002: relationship with soil moisture and effects of surface warming. *Journal of Hydrometeorology* **5**(6): 1117–1130. DOI: 10.1175/JHM-386.1
- Guttman NB. 1998. Comparing the Palmer drought index and the standardized precipitation index. *Journal of the American Water Resources Association* **34**(1): 113–121. DOI: 10.1111/j.1752-1688.1998.tb05964.x
- Guttman NB. 1999. Accepting the standardized precipitation index: a calculation algorithm. *Journal of the American Water Resources Association* **35**(2): 311–322. DOI: 10.1111/j.1752-1688.1999.tb03592.x
- Guttman NB, Wallis JR, Hosking JRM. 1992. Spatial comparability of the Palmer drought severity index. *Journal of the American Water Resources Association* **28**(6): 1111–1119. DOI: 10.1111/j.1752-1688.1992.tb04022.x
- Hayes MJ, Svoboda MD, Wilhite DA, Vanyarkho OV. 1999. Monitoring the 1996 drought using the standardized precipitation index. *Bulletin of the American Meteorological Society* **80**(3): 429–438. DOI: 10.1175/1520-0477(1999)080<0429:MTDUTS>2.0.CO;2
- Heddinghaus TR, Sabol P. 1991. A review of the Palmer drought severity index and where do we go from here? In *Preprints of the 7th Conference on Applied Climatology*, September 10–13, Salt Lake City, Utah; 242–246.
- Hosking JRM. 1990. L-moments: analysis and estimation of distributions using linear combinations of order statistics. *Journal of the Royal Statistical Society, Series B* **52**(1): 105–124.
- IPCC. 2007. Climate Change 2007: Synthesis Report. Contribution of Working Groups I, II and III to the Fourth Assessment Report of the Intergovernmental Panel on Climate Change, Core Writing Team, Pachauri RK, Reisinger A (eds). IPCC: Geneva, Switzerland; 104.
- Lloyd-Hughes B, Saunders MA. 2002. A drought climatology for Europe. *International Journal of Climatology* **22**(13): 1571–1592. DOI: 10.1002/joc.846
- Lorenzo-Lacruz J, Vicente-Serrano SM, López-Moreno JI, Beguería S, García-Ruiz JM, Cuadrat JM. 2010. The impact of droughts and water management on various hydrological systems in the headwaters of the Tagus River (central Spain). *Journal of Hydrology* **386**(1–4): 13–26. DOI: 10.1016/j.jhydrol.2010.01.001
- Ma MW, Song SB, Ren LL, Jiang SH, Song JL. 2013. Multivariate drought characteristics using trivariate Gaussian and Student *t* copulas. *Hydrological Processes* **27**(8): 1175–1190. DOI: 10.1002/hyp.8432
- McKee TB, Doesken NJ, Kleist J. 1993. The relationship of drought frequency and duration to time scales. In *Preprints of the 8th Conference on Applied Climatology*, January 17–22, Anaheim, California; 179–184.
- Palmer WC. 1965. Meteorological Drought. Research Paper No. 45. US Weather Bureau: Washington, DC; 58.
- Paulo AA, Rosa RD, Pereira LS. 2012. Climate trends and behaviour of drought indices based on precipitation and evapotranspiration in Portugal. *Natural Hazards and Earth System Sciences* **12**(5): 1481–1491. DOI: 10.5194/nhess-12-1481-2012
- Thornthwaite CW. 1948. An approach toward a rational classification of climate. *Geographical Review* **38**(1): 55–94. DOI: 10.2307/210739
- Vicente-Serrano SM, Beguería S, López-Moreno JI, Angulo M, Kenawy AE. 2010a. A new global 0.5° gridded dataset (1901–2006) of a multiscalar drought index: comparison with current drought index datasets based on the Palmer drought severity index. *Journal of Hydrometeorology* **11**(4): 1033–1043. DOI: 10.1175/2010JHM1224.1
- Vicente-Serrano SM, Beguería S, López-Moreno JI. 2010b. A multiscalar drought index sensitive to global warming: the standardized precipitation evapotranspiration index. *Journal of Climate* **23**(7): 1696–1718. DOI: 10.1175/2009JCLI2909.1
- Vicente-Serrano SM, López-Moreno JI, Beguería S, Lorenzo-Lacruz J, Azorin-Molina C, Morán-Tejeda E. 2012. Accurate computation of a streamflow drought index. *Journal of Hydrologic Engineering* **17**(2): 318–332. DOI: 10.1061/(ASCE)HE.1943-5584.0000433
- Vogel RM, Fennessey NM. 1993. L moment diagrams should replace product moment diagrams. *Water Resources Research* **29**(6): 1745–1752. DOI: 10.1029/93WR00341
- Webb RW, Rosenzweig CE, Levine ER. 2000. Global soil texture and derived water-holding capacities data. Available from: <http://www.daac.ornl.gov> (accessed October 2012).
- Wells N, Goddard S, Hayes MJ. 2004. A self-calibrating Palmer drought severity index. *Journal of Climate* **17**(12): 2335–2351. DOI: 10.1175/1520-0442(2004)017<2335:ASPDSI>2.0.CO;2
- Zhang L. 2005. Multivariate hydrological frequency analysis and risk mapping. Ph.D. thesis, Louisiana State University; 408.